J. Plasma Physics (2001), *vol.* 65, *part* 2, *pp.* 107–129. Printed in the United Kingdom
© 2001 Cambridge University Press

Ion phase-space vortices in 2.5-dimensional simulations

STEINAR BØRVE,[1] HANS L. PÉCSELI[2] and JAN TRULSEN[1]

[1]Institute for Theoretical Astrophysics, University of Oslo, Box 1029, Blindern, N-0315 Oslo, Norway

[2]Physics Department, University of Oslo, Box 1048, Blindern, N-0316 Oslo, Norway

(Received 27 March 2000 and in revised form 27 May 2000)

Abstract. The formation and propagation of ion phase-space vortices are observed in a numerical particle-in-cell simulation in two spatial dimensions and with three velocity components. The code allows for an externally applied magnetic field. The electrons are assumed to be isothermally Boltzmann-distributed at all times, implying that Poisson's equation becomes nonlinear for the present problem. Ion phase-space vortices are formed by the nonlinear saturation of the ion–ion two-stream instability, excited by injecting an ion beam at the plasma boundary. We consider the effect of a finite beam diameter and a magnetic field, in particular. A vortex instability is observed, appearing as a transverse modulation, which slowly increases with time and ultimately breaks up the vortex. When many vortices are present at the same time, we find that it is their interaction that eventually leads to a gradual filling-up of the phase-space structures. The ion phase-space vortices have a finite lifetime, which is noticeably shorter than that found in one-dimensional simulations. An externally imposed magnetic field can increase this lifetime considerably. For high injected beam velocities in magnetized plasmas, we observe the excitation of electrostatic ion-cyclotron instabilities, but see no associated formation of ion phase-space vortices. The results are relevant, for instance, for the interpretation of observations by instrumented spacecraft in the Earth's ionosphere and magnetosphere.

1. Introduction

Analytical studies have demonstrated that collisionless plasmas as described by the Vlasov equation formally allow a large class of nonlinear equilibrium states: BGK modes. The original studies referred to one spatial dimension (Bernstein et al. 1957), but later (Kato 1976; Ishibashi and Kitahara 1992) these results were generalized to two and three spatial dimensions, although with imposed symmetry conditions. Theoretically, the phase-space dynamics of electrons and ions can support a surprisingly rich variety of electrostatic structures. In reality, relatively few types are observed – here we shall only be concerned with so-called phase-space vortices. The formation of such states was observed first in numerical simulations (Berk et al. 1970), and later in a series of laboratory experiments. The first of these experiments relied on ideas and an excitation mechanism conceived and tested by Koichi Saéki.

https://doi.org/10.1017/S0022377801008947 Published online by Cambridge University Press

The first experimental results were reported by Saéki (1973), with detailed experimental observations carried out later in a strongly magnetized plasma in the Risø Q-machine by Saéki et al. (1979). A detailed discussion also including numerical simulations was later presented by Lynov et al. (1979), see also the review by Schamel (1986). These first experiments dealt with phenomena on the short timescales where the ion component could be considered immobile. Similar vortical structures were found numerically (Sakanaka 1972; Pécseli et al. 1984) and experimentally (Pécseli et al. 1981, 1984) also in ion phase space. In this experiment, the ion phase-space dynamics were studied directly using an ion energy analyser; see also the summary by Pécseli (1984). Other experiments later confirmed some of these observations (see e.g. Chan et al. 1984), but investigated only space–time variations of plasma density and potential. Evidence for the formation, propagation and subsequent decay of phase-space vortices was also obtained in experiments carried out in an unmagnetized double-plasma device (Johnsen et al. 1985, 1987), where an ion beam was injected into a background plasma, using a conditional sampling method for analysing the space–time variation of the spontaneously generated fluctuations in plasma density. Recent observations by Nakamura et al. (1999) also show the formation and propagation of 'ion holes', i.e. ion phase-space vortices. These experiments were carried out under conditions similar to those in the studies by Pécseli et al. 1981, 1984), but with larger electron-to-ion temperature ratios.

Phase-space vortices seem to be a generic feature of the saturated stage of beam–plasma instabilities (Kako et al. 1971; Pécseli and Trulsen 1982) – at least in one spatial dimension – indicating that this saturated stage can be considered as a relatively low-dimensional system, described by a random superposition of such coherent structures together with a low-level noise component (Kofoed-Hansen et al. 1989). (It is an interesting, but unresolved, question whether this noise is additive or multiplicative.) Phase-space vortices can, however, be excited by other means as well, short particle bursts for instance, and not necessarily only by beam instabilities.

The processes determining the lifetime of phase-space vortices in one, two and three spatial dimensions are not well understood: in studies of the nonlinear evolution of electron two-stream instabilities, Morse and Nielson (1969) found that such vortices had a very long lifetime in one dimension, disintegrated slowly in two dimensions, and disappeared quite rapidly in three dimensions for unmagnetized plasmas, although not much was learned concerning the *nature* of the processes that lead to the destruction of the phase-space vortices. It might be that an externally imposed magnetic field prolongs the vortex lifetime, but numerical simulations of electron vortices (Oppenheim et al. 1999) show also in this case a breakup of vortex structures. Fijalkow (1999) observed that an externally imposed magnetic field reduced the lifetime of electron vortices (with immobile ions), but this observation refers to a restricted geometry. We recall here that the experimental observation of electron vortices reported by Saéki et al. (1979) were actually obtained in magnetized plasmas, with strong magnetic fields, $\omega_{ce} > \omega_{pe}$.

It is not evident that the conclusions from electron-beam instabilities can be generalized immediately to ion–ion-beam instabilities, because in this latter case the one-dimensional case is only weakly dispersive, and directional dispersion of ion-beam-generated waves is only significant for high beam velocities. One motivation for our study was to also investigate this question with the numerical plasma simulation to be described. (The preceding discussion deals with the full conditions

https://doi.org/10.1017/S0022377801008947 Published online by Cambridge University Press

for the excitation of phase-space vortices, and has little to do with the actual stability of an *individual* vortex; the appropriate stability analysis has been investigated by, for example, Schamel (1982) and Turikov (1984).) Also, the study of Morse and Nielson (1969) refers to an initial condition where the beams are present all over space; this is not the most experimentally relevant case. We wanted to study an experimentally more realistic condition, where a beam is injected at the boundary of a pre–existing background plasma. The analysis is restricted to electrostatic phenomena occurring on time scales below the ion plasma frequency. In this case, we can assume that the electrons are isothermally Boltzmann-distributed at all times. This simplification is obtained at the expense of a nonlinear Poisson equation

$$\nabla^2 \Phi(\mathbf{r}, t) = \frac{e n_0}{\varepsilon_0} \left(e^{e\Phi(\mathbf{r},t)/T_e} - \frac{n(\mathbf{r}, t)}{n_0} \right) , \tag{1}$$

in terms of the electron temperature T_e, the ion density n and the electrostatic potential ϕ. Charge conservation within this model implies

$$\int \left[n_0 \exp\left(\frac{e\Phi(\mathbf{r}, t)}{T_e} \right) - n(\mathbf{r}, t) \right] dx\, dy = 0.$$

The approach based on (1) has some obvious advantages. First, we avoid the unphysical electron-to-ion mass ratios that are often employed to reduce computer requirements. Secondly, we can readily identify the specific ion phase-space dynamics important for the observed time evolutions. The cost incurred with this model is obviously that the electron phase-space information is lost. This information would be crucial, for instance, for electron–ion streaming velocities, so this and similar phenomena are excluded from our analysis. We note that in the case of high electron-to-ion temperature ratios, a parameter range exists where electron collisionality is important while ions can be considered collisionless. In this case, our basic assumption is easily justified. Since we want to be able to consider arbitrary length scales, we do *not* assume quasineutrality from the outset.

This paper deals primarily with the results of numerical simulations; essential details of the numerical methods used are summarized in an appendix.

2. Numerical results

Our study can conveniently be separated into two parts: magnetized and unmagnetized plasmas. In the latter case, we do not actually need the possibility of full three-dimensional motion of ions, but it is included nevertheless. For magnetized plasmas, all the ions perform a gyrating motion along the magnetic field, which is parallel to the computational plane, but the plasma density and potential do not vary along the third spatial coordinate. A summary of the parameters for the different simulations is shown in Table 1, with V_b/v_{th} being the ratio of ion-beam velocity and background ion thermal velocity, while n_b/n_B is the ratio of ion beam to background densities. In this paper, we present results for selected electron-to-ion temperature ratios. In particular, we have studied $T_e/T_i = 40$. For this case, we have that the sound speed defined as $C \equiv \sqrt{(T_e + 3T_i)/M}$ is approximately $C = 6.6\, v_{\mathrm{th}}$. The temperature ratio of the ion beam to background was constant: $T_{b\|}/T_i = \frac{1}{3}$ and $T_{b\perp}/T_i = 1$. The size of the simulation domain in most cases considered here is a rectangle with sides $100\,\lambda_D/\sqrt{2}$ and $250\,\lambda_D/\sqrt{2}$, where λ_D is the electron Debye length (the number $\sqrt{2}$ originates from a convenient choice of ref-

https://doi.org/10.1017/S0022377801008947 Published online by Cambridge University Press

Table 1. Summary of simulation parameters and vortex properties, where $v_{\rm th} \equiv \sqrt{T_i/M}$ and $C_s \equiv \sqrt{T_e/M}$.

Beamwidth λ_D	Ω_{ci}/ω_{pi}	$V_b/v_{\rm th}$	V_b/C_s	n_b/n_B	$\Delta Y/\lambda_D$	$\Delta U/C_s$	Vortex lifetime ω_{pi}^{-1}
$T_e/T_i = 10$							
Full beam	0	6.7	2.12	0.2	10 ± 1.5	1.5 ± 0.5	Uncertain
20	0.5	6.7	2.12	0.2	—	—	—
$T_e/T_i = 20$							
Full beam	0	6.7	1.50	0.2	4.4 ± 0.4	1.3 ± 0.2	50 ± 10
20	0.5	6.7	1.50	0.2	5.3 ± 0.8	1.3 ± 0.2	60 ± 20
$T_e/T_i = 40$							
Full beam	0	6.7	1.06	0.2	3.2 ± 0.8	0.9 ± 0.2	20 ± 10
20	0	6.7	1.06	0.2	3.6 ± 0.8	1.0 ± 0.2	30 ± 15
20	0.1	6.7	1.06	0.2	3.4 ± 0.6	0.9 ± 0.3	30 ± 10
60	0.1	6.7	1.06	0.2	3.5 ± 1.0	0.9 ± 0.3	40 ± 10
20	0.5	6.7	1.06	0.2	3.6 ± 0.6	1.0 ± 0.2	60 ± 20
60	0.5	6.7	1.06	0.2	3.5 ± 1.0	0.9 ± 0.3	60 ± 15
20	1	6.7	1.06	0.2	3.8 ± 0.5	1.0 ± 0.2	>150

erence temperature for both electrons and ions, in order to improve the stability of the numerical code, implying a length unit in the simulations of $\lambda_D/\sqrt{2}$). The total number of background simulation particles was 13×10^6, the beam particles come in addition, with a number varying according to the distance the beam has penetrated, given the ratio n_b/n_B. The case where the beam had the full simulation width is indicated by 'Full beam' in the table. For $T_e/T_i = 10$ and $\Omega_{ci}/\omega_{pi} = 0.5$, no vortices are formed, and in this case we find that the plasma is stable with respect to the ion-beam instability. The indicated scatters in the results originate in part from variations observed from different simulations with different initializations of random-number generators and in part from scatter in parameters describing different vortices in the same realization.

2.1. Unmagnetized plasmas

As a reference case, we assumed that the initial condition was one-dimensional, i.e. an ion beam is injected in the full cross-section of the simulation plasma. The simulation, however, allows fluctuations to develop from the noise due to particle

Figure 1. (a) An example of a realization for the ion phase-space density in the (x, y) plane at selected times, with points corresponding to simulation particles in the velocity interval $(0.27 \pm 0.05)\sqrt{T_e/M}$. The shock front is outside the top of the frames. (b) The phase-space density at selected times. In the present case, we show the y-component of the velocity taken along the y-axis at $x = 0$ within an interval of $2\sqrt{2}\lambda_D$ in this and the following cases. Note the moving frames. We have $T_e/T_i = 40$ and $\Omega_{ci} = 0$.

https://doi.org/10.1017/S0022377801008947 Published online by Cambridge University Press

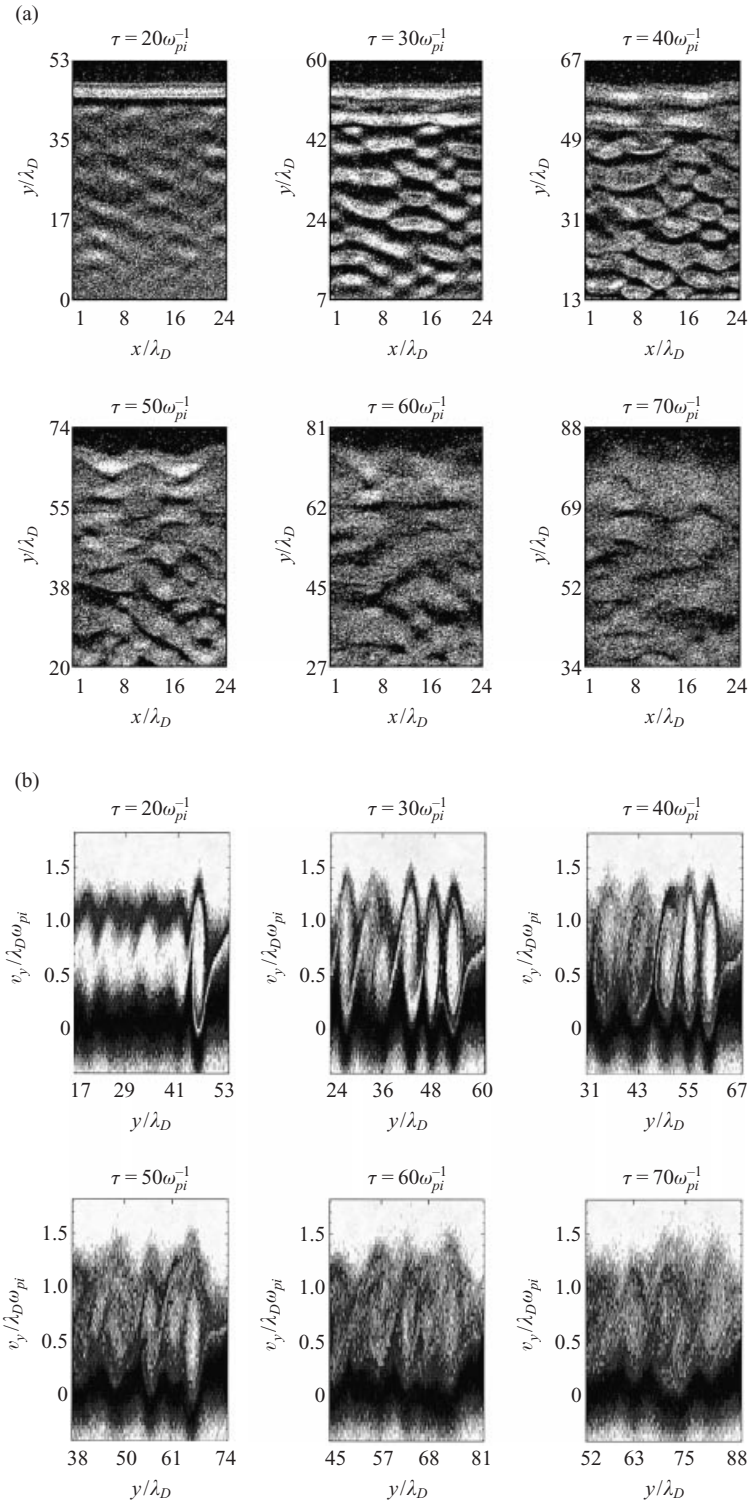


Figure 1. For caption see facing page.

https://doi.org/10.1017/S0022377801008947 Published online by Cambridge University Press

discreteness in the two spatial dimensions. We show results for the reference case in Fig. 1. Note that the frames are moving to follow the beam front. In Fig. 1(a), we show a two-dimensional slab in the ion phase space at selected times in the full (x, y) plane. The white regions have a low particle density, which corresponds to localized depletions in the bulk plasma density. The space–time variation of the ion density is not trivially derived from the potential, since our model retains the full nonlinear Poisson equation with Boltzmann-distributed electrons. We find that the additional information in the ion density and potential is not sufficient to warrant the inclusion of one more figure.

Figure 1(b) shows the particle density in ion phase space along a selected axis (here, the beam direction) in the simulation at selected times. We show particle density obtained at these selected times by averaging small pixels of width $0.14\,\lambda_D$ along the beam axis, and a velocity interval of $0.22\,v_{\rm th}$ in the same direction, and $2.8\,\lambda_D$ in the beam-transverse direction. For a given direction of the selected axis, we can construct the phase space by selecting any direction for the velocity, i.e. the figure *need* not present the distribution of the ion velocity component along the same direction as that of the selected axis.

In our results, we find the initial evolution to be quite similar to that found by Sakanaka (1972), who solved the one-dimensional Vlasov equation, and by Pécseli et al. (1984), who used a particle-in-cell (PIC) code. We note the formation of a shock front (Ikezi et al. 1973), and behind it a number of phase-space vortices noticeable as potential wells and corresponding vortical configurations in phase-space. The formation time of a phase-space vortex is for the present case approximately $20\omega_{pi}^{-1}$; this is the time it takes to merge the ion beam with the background plasma at two regions surrounding a vortex. The vortex-formation time in beam–plasma systems is not related to the bounce period of charged particles in potential wells.

In a phase space spanned by x, y and v_y, we observe that the phase-space vortex is associated with a 'tube-like' structure, which is inconspicuous in an (x, y, v_x) space, the beam direction being in the y direction. The formation time, lifetime, spatial widths and peak density perturbations associated with the phase space vortices agree reasonably well with the observations reported by Pécseli et al. (1984).

For large times, we find that vortex structures in phase space are slowly eroding, and we can estimate an upper limit for the lifetime of approximately $40\omega_{pi}^{-1}$. With a peak potential depletion of $\phi_m \approx 0.2\,T_e/e$ and a typical width at half peak amplitude of a potential well of $\mathscr{L} \approx 3.5\lambda_D$ in terms of the electron Debye length, we can estimate the ion bounce frequency as $\sqrt{(e/M)\phi_m/\mathscr{L}^2} \approx 0.1\,\omega_{pi}$, or a bounce time as approximately 9 ion plasma periods $2\pi/\omega_{pi}$, implying that the lifetime of an observed phase-space vortex is somewhat larger than the ion bounce period in this case. The estimate for the lifetime of ion phase-space vortices given by Johnsen et al. (1985), was approximately 50 ion plasma periods $2\pi/\omega_{pi}$, obtained in a laboratory experiment in unmagnetized plasmas, where the full three-dimensional evolution of the structures could take place. The bounce frequency in that experiment was only $0.01\omega_{pi}$ and the hole width was approximately $100\,\lambda_D$ at the base, and close to $50\,\lambda_D$ at half amplitude. The temperature ratio was, however, approximately 10, i.e. considerably smaller than here.

The spatial width $\mathscr{L}$ of the vortices, as well as their depth ϕ_m, had a non-trivial variability in time as well as from one vortex to another. We found no correlation, however, between $\mathscr{L}$ and ϕ_m, and there is no theoretical basis (Bernstein et al. 1957) to expect one either.

https://doi.org/10.1017/S0022377801008947 Published online by Cambridge University Press

The density and phase-space variations shown give an overall qualitative impression of the space–time evolution of coherent structures in our system. In order to obtain quantitative information, we performed a singular-value decomposition of the density variation, but found that such an analysis was of little use in the present context, since it mixed information concerning coherent structures in the form of phase-space vortices with other types of perturbations that were present – the beam front in particular. The singular-value decomposition was made useful only by limiting the area of analysis to contain nothing but a vortex. Since in that case the vortex had to be identified by other means in advance, we found this procedure to add little of significance.

In the present study, we identify vortices by making a narrow cut in phase space in a direction parallel to the beam velocity. In this selected region of phase space, we find a local minimum of the particle density in a velocity region specified to be within the interval between the background thermal velocity and the beam velocity. Around such a point, we fit an ellipse to the full phase-space density variation at the maximum phase-space gradient. A phase-space vortex can then be identified, and the major and minor axis in the ellipse give a measure of its spatial width ΔY and the trapping width ΔU. A local minimum is rejected as a candidate for a phase-space vortex in cases where the search for a local phase-space gradient shows that the minimum found is not completely surrounded in phase space, as evidenced by a poor fit of the ellipse. In Fig. 2, we show the time evolution of phase-space vortices identified by this method. The results are expressed in length units of λ_D and velocity units $\lambda_D\omega_{pi} \equiv \sqrt{T_e/M}$. The units chosen for velocity are the most convenient, given the units for time and length. The unit for trapping width ΔU is evidently related to the potential depth associated with the ion phase-space vortex.

A termination of a line in Fig. 2, for example for ΔU, means that the vortex could no longer be identified at this position. This can imply either that the vortex has eroded beyond recognition or that it has merged with another vortex to have its position at a different place. The somewhat non-standard vortex-fitting method described here has some advantages as compared with measuring widths and amplitudes on a presentation of for instance $n(\mathbf{r}, t)$, since in most cases it will be difficult to define a base-line to use as reference in the latter case. The values we obtain for ΔY, for instance, will be smaller (typically one-third) of the value estimated from the density variation by taking the distance between the two 'shoulders' of the density depletion.

A number of the simulations were repeated with different initializations of the random-number generators, giving a modification of the initial noise level due to the discrete particles, all macroscopic parameters being the same. We observed that the resulting phase-space variation was surprisingly sensitive to the initial noise – an observation that actually has some analytical support, as discussed by Pécseli et al. (1984). Only the characteristics of the first phase-space vortex (the one immediately behind the collisionless shock), were to a large extent reproducible, irrespective of the particle noise. When quoting a vortex-formation time, we refer to this vortex. However, this vortex need not be the one that survives for the longest time in *every* realization. The distribution and characteristics of the trailing vortices could vary significantly when the initialization of the particle distributions was changed.

The basic and most important features of the results for the full beam shown in Figs 1 and 2 can be summarized as follows. The vortex immediately trailing the shock front forms first, and is initially quite uniform in the direction along

https://doi.org/10.1017/S0022377801008947 Published online by Cambridge University Press

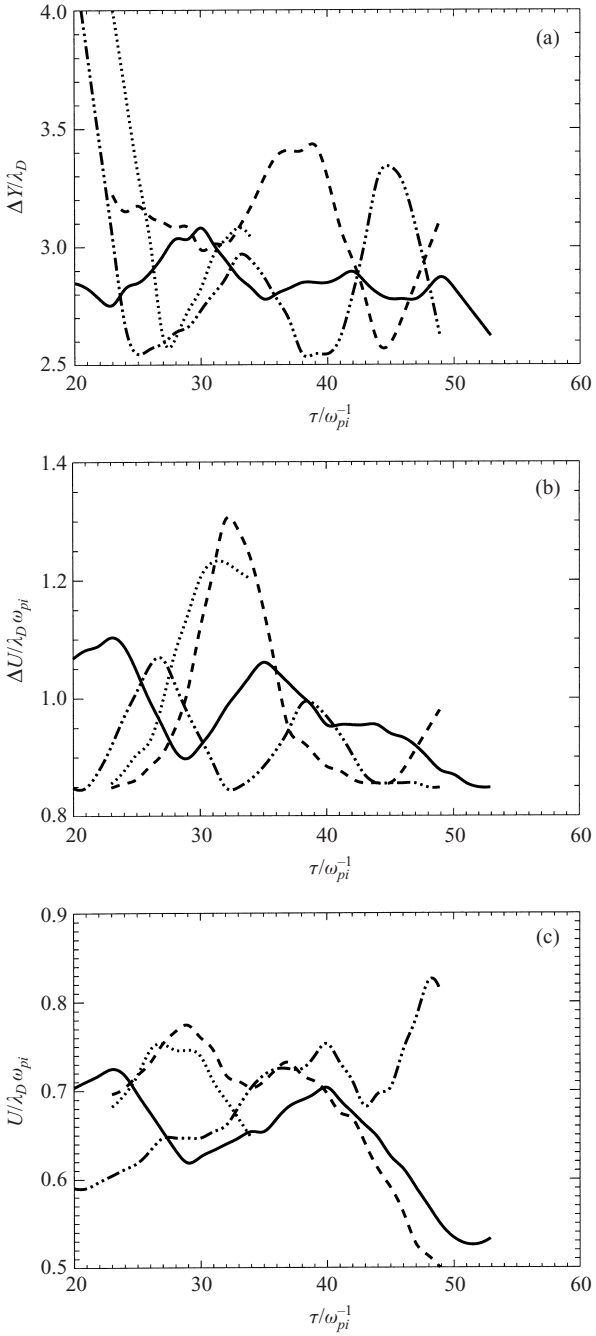


Figure 2. Time evolution of (a) the widths ΔY, (b) the amplitudes ΔU and (c) the velocities U of ion vortices. The vortices are identified by the phase-space ellipse-fitting method.

the shock. It is followed by other vortices developing somewhat more slowly, and these are somewhat irregular from the very beginning, being of finite length in the direction parallel to the shock and with axes slightly misaligned with respect to the shock front. This observation is consistent with an interpretation where vortices

https://doi.org/10.1017/S0022377801008947 Published online by Cambridge University Press

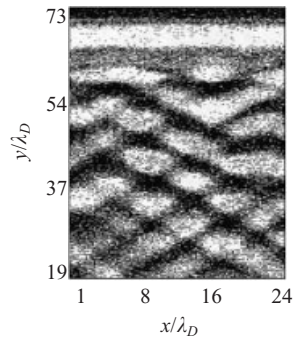


Figure 3. Ion phase-space density in the (x, y) plane for a selected time $40\,\omega_{pi}^{-1}$, to be compared with Fig. 1(a), here points correspond to simulation particles in the velocity interval $(0.39 \pm 0.05)\,\sqrt{T_e/M}$. We have $T_e/T_i = 20$ and $\Omega_{ci} = 0$.

develop by the ion–ion two-stream instability (Fried and Wong 1966; Kiwamoto 1974; Grésillon and Doveil 1975), i.e. the orientation of the first vortex is imposed by the shock, while the following vortices develop in a cone of directions within the cone spanned by the wave vectors of the linearly unstable waves. The subsequent time evolution of the saturated vortices differs for the front and the trailing ones. For the first vortex, we note a slight kink and a stronger 'sausage' perturbation developing. We note that the shock remains strictly planar in comparison, so this vortex modulation is spontaneous, and not imposed by variation in the shock front. The modulation of the vortex increases aperiodically, the sausage perturbation increasing most rapidly. The aperiodic vortex instability was predicted by Schamel (1982). We estimate a characteristic time scale to be approximately $20/\omega_{pi}$, with the scale length of the most unstable perturbation being approximately $15\lambda_D$. These values are comparable to the theoretical results (Schamel 1982). The growth rate of this instability decreases with decreasing T_e/T_i, while the most unstable length scale increases. It is not possible to obtain any accurate quantitative measure for the growth rates or scale lengths.

For the trailing ion vortices, we find a different temporal evolution. Here, the dominant feature is local merging between two vortices, until finally a sparse 'vortex net' is formed, resembling 'wormholes' in phase space. These complicated structures open channels for particles to move into and eventually fill up the vortices from the ends, and we see them decay, or rather disintegrate. The merging or coalescence of vortices can be observed, but does not seem to be an important process for the dynamics in this unmagnetized case.

Pécseli et al. (1984) expected that the experimentally observed limitations on the lifetime of phase-space vortices were due mainly to ion–neutral collisions, charge exchange collisions in particular. It was demonstrated numerically that these collisions could indeed disintegrate an ion phase-space vortex, but the present numerical results demonstrate that even in purely collisionless plasmas we find a lifetime comparable to that observed experimentally.

To substantiate the relation between the linear ion–ion beam instability and the formation of ion phase space vortices, we show in Fig. 3 a selected time step from a simulation with $T_e/T_i = 20$, and other parameters as in Figs 1 and 2; see also Table 1. We note the clear inclination of the vortex axes, which are at an

https://doi.org/10.1017/S0022377801008947 Published online by Cambridge University Press

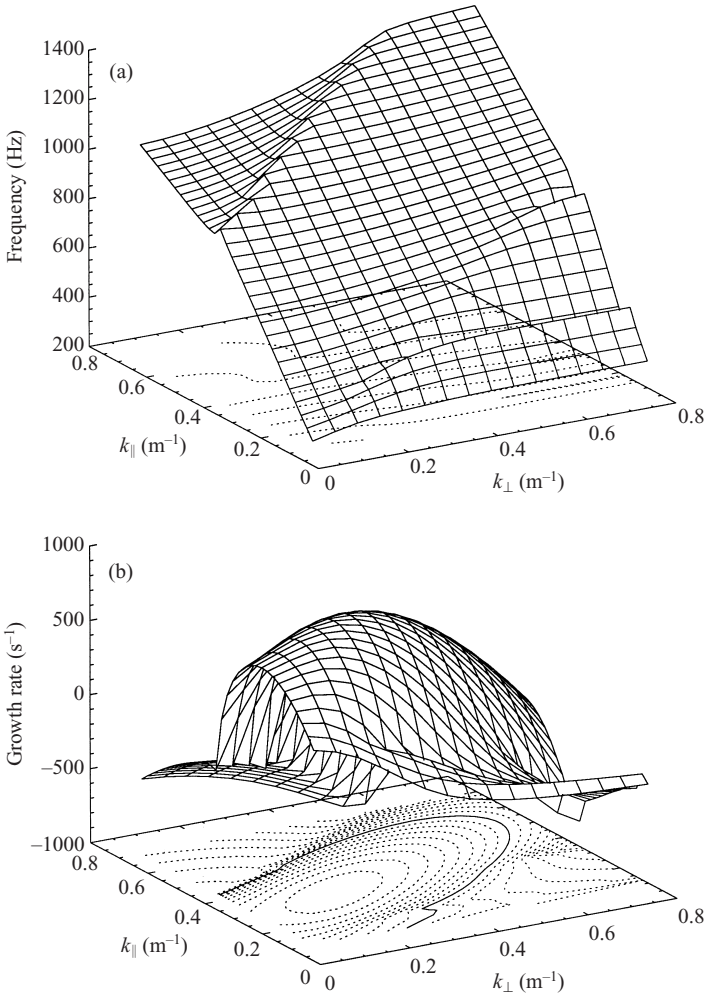


Figure 4. Dispersion relation obtained by numerical solution. The real part of the dispersion relation $\omega = \omega(\mathbf{k})$ as a function of $(k_\perp, k_\parallel)$ is shown in (a) and the imaginary part in (b). Our code for solving the dispersion relation assumes that parameters are entered for a physical condition, so we have chosen parameters such that $2\pi\omega_{pi} = 1$ kHz for simplicity. Relative values for the beam and background plasma parameters are as in Table 1 for $T_e/T_i = 20$ and $\Omega_{ci} = 0$. With these parameters, we have $k = 0.5$ corresponding here to a wavelength of $4.4\,\lambda_D$.

angle of approximately 45° to the direction of the beam propagation. We have solved the full linear plasma dispersion relation (Nicholson 1983) numerically, and obtained the results shown in Fig. 4, which clearly demonstrate that the linearly most unstable waves propagate at an angle of approximately 53° to the direction of beam propagation, close to the value deduced from Fig. 3. Some small 'fringes' in the dispersion relation shown in Fig. 4 at large $k_\perp$ and small $k_\parallel$ are due to several competing zeros of the dielectric function with nearly identical imaginary parts of the frequency. For short wavelengths, we have in principle three primary modes: the fast and slow beam modes and an acoustic branch (Grésillon and Doveil 1975), where the two latter merge in the unstable region. In addition, we have higher-

https://doi.org/10.1017/S0022377801008947 Published online by Cambridge University Press

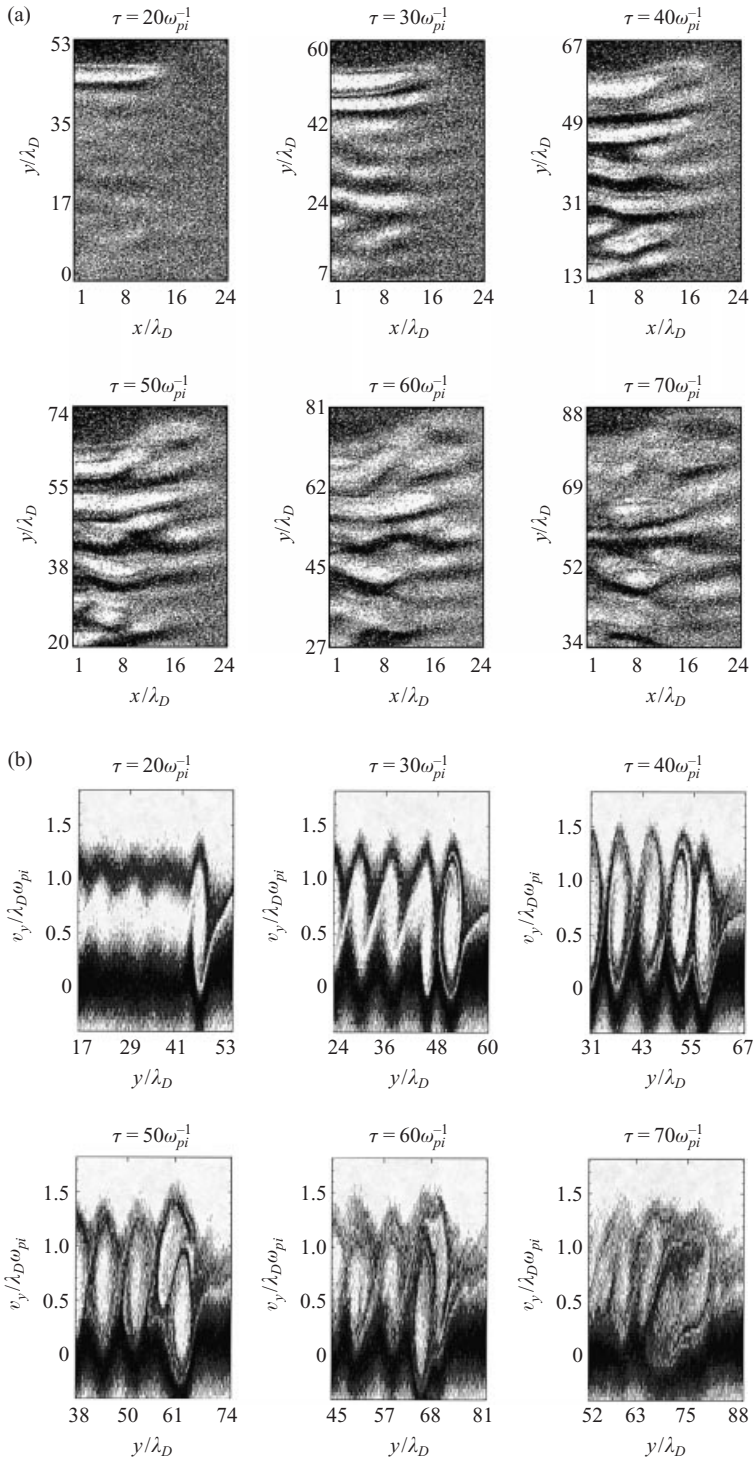


Figure 5. Ion phase-space density for selected times, for a finite ion beam diameter, to be compared with Fig. 1; here, in (a), points correspond to simulation particles in the velocity interval $(0.3 \pm 0.05)\sqrt{T_e/M}$. We have $\Omega_{ci} = 0$.

https://doi.org/10.1017/S0022377801008947 Published online by Cambridge University Press

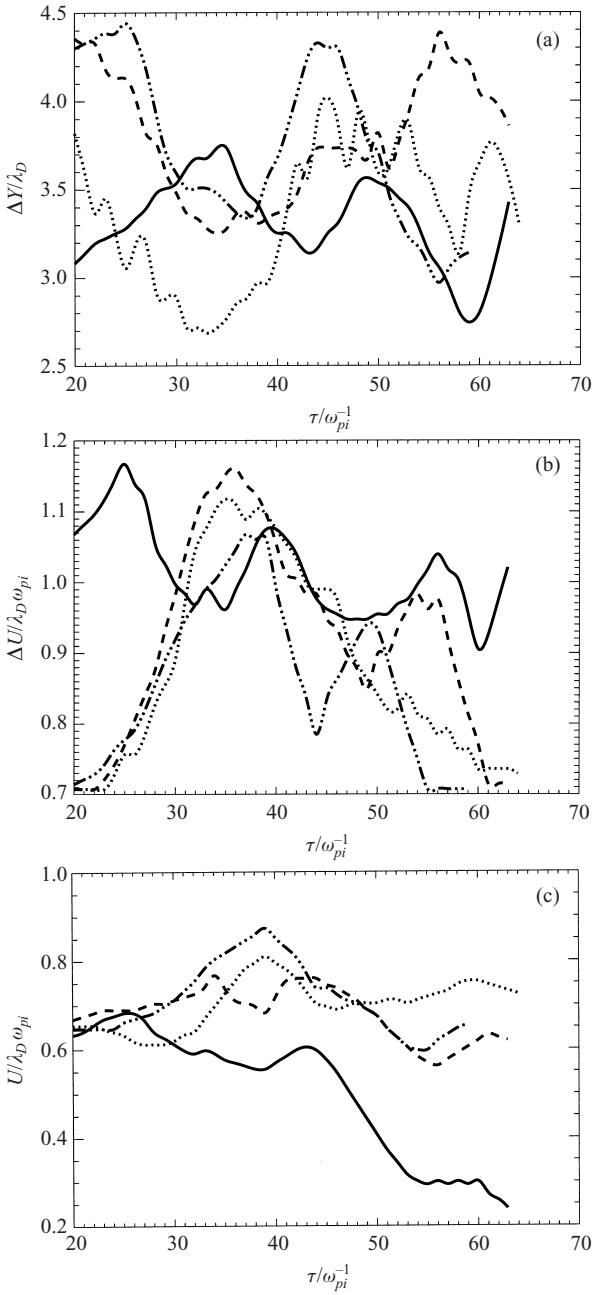


Figure 6. Time evolution of (a) the widths ΔY, (b) the amplitudes ΔU and (c) the velocities U of ion vortices, as identified for finite ion-beam cross-section by the phase-space ellipse-fitting method as in Fig. 2.

order modes originating from strongly damped solutions of the dispersion relation. The dispersion relation shown in Fig. 4 is continued as the acoustic branch in our representation. The fast beam mode is damped for all wavenumbers, and is not shown here.

https://doi.org/10.1017/S0022377801008947 Published online by Cambridge University Press

In general, the linearly most unstable wavelength increases as the electron temperature is decreased, with all other parameters being constant. This property is consistent with the results summarized in Table 1. For further details concerning the ion–ion-beam instabilities, we refer to Fried and Wong (1966), Kiwamoto (1974) and Grésillon and Doveil (1975).

2.1.1. Finite beam diameter. In order to reduce the effect of the transverse instability, we have carried out simulations with a finite beam diameter. In Figs 5(a,b), we show examples of the ion phase-space density at selected times, with the same form of presentation as in Fig. 1. In Fig. 6, we show the time evolution of the corresponding vortex parameters, as in Fig. 2. The vortices are now well localized in the x as well as the y direction, to form elliptical depletions in plasma density. The front vortex has a width close to the beam width; the trailing ones can be similar or show a bifurcation, forming as two holes that are symmetric with respect to the beam axis.

We find that the instability of the front vortex is indeed suppressed in the sense that its lifetime is now controlled by the same mechanism as for the trailing vortices. The vortex lifetimes deduced from Fig. 6 are very close to those from Fig. 2.

2.2. Magnetized plasmas

In order to reduce the effect of ion diffusion into the vortex along the vortex axis, we have repeated the analysis described in Sec. 2.1, now taking into account an externally imposed homogeneous magnetic field. This field is assumed to be of sufficient intensity to allow the fluctuations to be described as electrostatic also in the nonlinear saturated stage. The key parameter in the present context is the ratio of ion plasma to ion cyclotron frequencies, Ω_{ci}/ω_{pi}. Considering the case where the ion-beam diameter is $20\lambda_D$ and $\Omega_{ci}/\omega_{pi} = 1$, we find that the results for the density and potential variations along the beam axis are almost indistinguishable from those of a purely one-dimensional simulation.

For a detailed analysis, we keep the beam diameter fixed, and vary Ω_{ci}/ω_{pi}. Results for the time evolution of one realization of the ion phase-space density are shown in Figs 7 and 8, for the case where $\Omega_{ci}/\omega_{pi} = 0.5$. In Fig. 7(b), we clearly note a coalescence of vortices – a process that is well known from simulations restricted to one spatial dimension. Evidently, the externally imposed magnetic field is here sufficient to recover this feature also in our 2.5-dimensional simulation.

The density depletions and characteristic widths of the observed phase-space vortices in the direction of the magnetic field do not depend on the magnetic field intensity. They appear to be controlled by basic plasma parameters such as temperatures and beam velocities, in the same way as for an unmagnetized plasma. The vortex scale length in the direction perpendicular to the beam velocity and magnetic field is determined solely by the diameter of the injected ion beam, provided that the beam diameter is much larger than the ion Larmor radius. We have the ion Larmor radius defined as $r_L \equiv \sqrt{T_i M}/eB$ being equal to the electron Debye length when $\omega_{pi} = \Omega_{ci}\sqrt{T_e/T_i}$, or $\Omega_{ci} \approx \frac{1}{6}\omega_{pi}$ in our case with $T_e/T_i = 40$.

We note that for finite beam widths, the fluctuations *in*side the beam couple to the plasma *outside* for the magnetized as well as for the unmagnetized case. This feature can be interpreted as a sort of 'radiation' induced by the coupling of the high-velocity fluctuations generated by the beam to the acoustic modes in the background plasma, as anticipated by, for instance, Huld et al. (1990).

https://doi.org/10.1017/S0022377801008947 Published online by Cambridge University Press

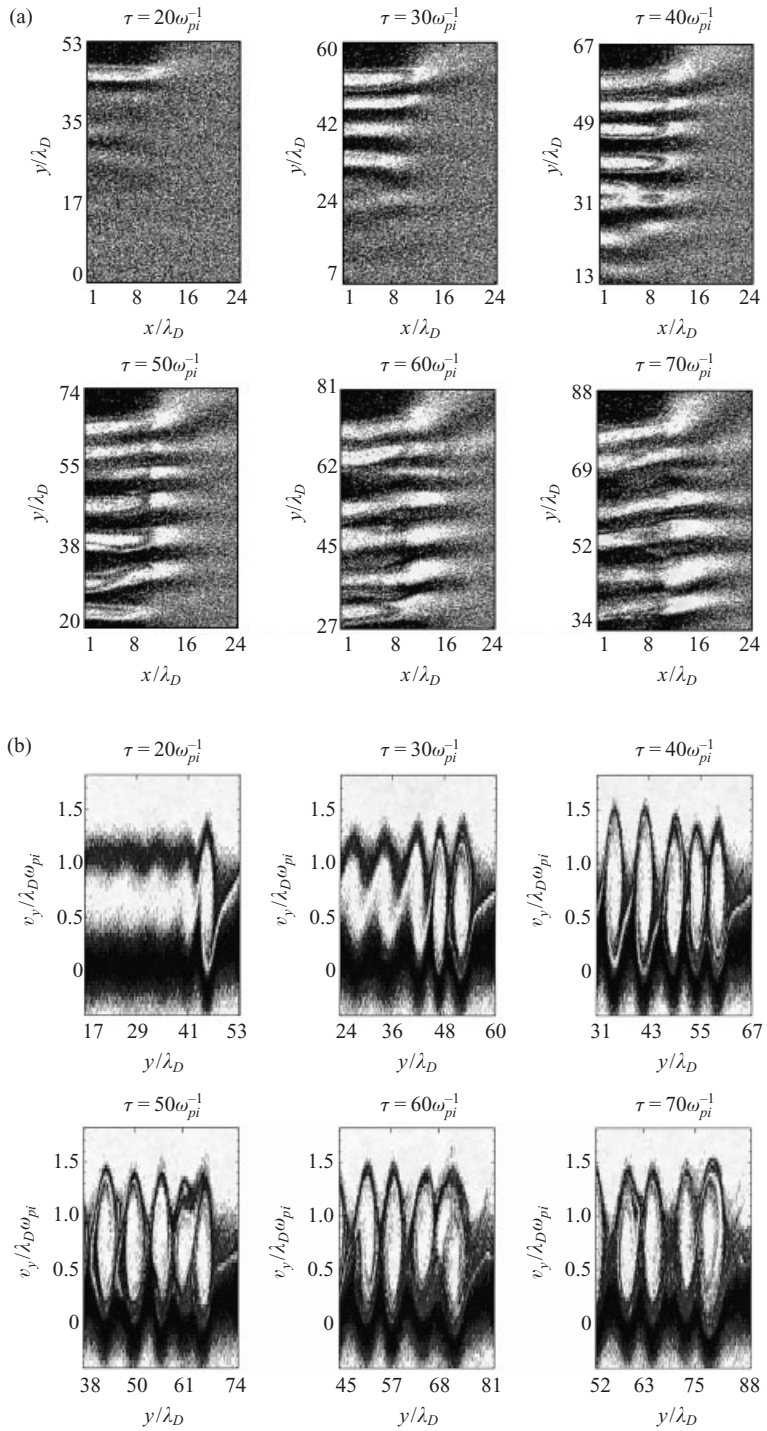


Figure 7. (a) The ion phase space density in the (x, y) plane for selected times, for a finite ion beam diameter in a magnetized plasma, to be compared with Fig. 1(a); here points correspond to simulation particles in the velocity interval $(0.3 \pm 0.05)\sqrt{T_e/M}$. (b) The phase space density at selected times, to be compared with Fig. 1(b). We have $\Omega_{ci}/\omega_{pi} = 0.5$.

https://doi.org/10.1017/S0022377801008947 Published online by Cambridge University Press

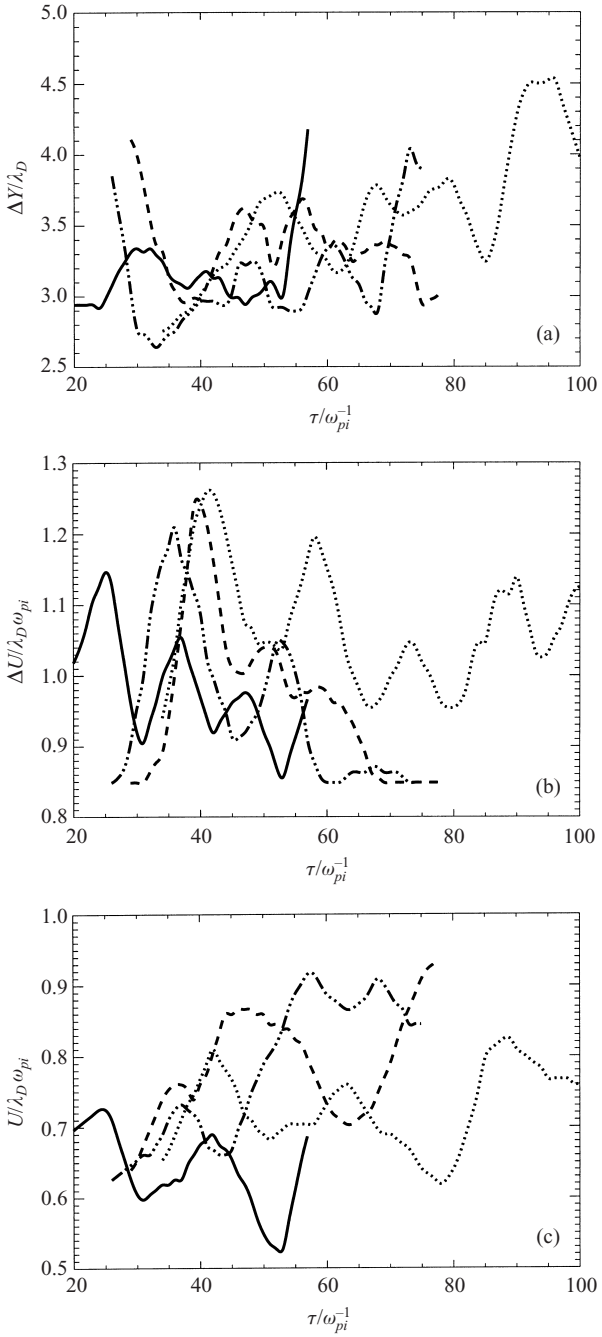


Figure 8. Time evolution of (a) the widths ΔY, (b) the amplitudes ΔU and (c) the velocities U of ion vortices, for the magnetized case as in Fig. 7.

We have also considered high injected beam velocities in magnetized plasmas, using velocities $10\,v_{\rm th}$ as well as $20\,v_{\rm th}$. In these cases, we observe the excitation of electrostatic ion cyclotron instabilities, but see no formation of ion phase-space vortices, thus emphasizing our preference for an interpretation of the ion acoustic

https://doi.org/10.1017/S0022377801008947 Published online by Cambridge University Press

instability as being responsible for the observed vortex formation. The beam excitation of the ion cyclotron instability is interesting in its own respect, and details will be reported in another paper.

2.2.1. BGK solutions in strongly magnetized plasmas. The existence of BGK equilibria in one spatial dimension is well known, and various scenarios for their formation is understood, although this question has subtle details that deserve further scrutiny. Generalizations of the BGK–type solutions have been considered for unmagnetized plasmas for two and three spatial dimensions (Kato 1976; Ishibashi and Kitahara 1992), but with imposed symmetry conditions. Stationary solutions in magnetized plasmas with immobile ions were discussed by Terry et al. (1990).

In a full *three-dimensional* system with a magnetic field, such structures can form long lived quasi-equilibria. Nonlinear BGK equilibria can for magnetized plasmas be constructed trivially from the Vlasov equation in its appropriate form, i.e. the drift kinetic equation

$$\frac{\partial f}{\partial t} + \boldsymbol{\nabla}_\perp \cdot (\mathbf{v}_\perp f) + v_z \frac{\partial f}{\partial z} - \frac{e}{M}\left(\frac{\partial}{\partial z}\boldsymbol{\Phi}\right)\frac{\partial f}{\partial v_z} = 0, \tag{2}$$

with

$$\mathbf{v}_\perp = \left[-\boldsymbol{\nabla}_\perp \boldsymbol{\Phi} \times \hat{\mathbf{b}} - \boldsymbol{\Omega}_{ci}^{-1} \boldsymbol{\nabla}_\perp \left(\frac{\partial \boldsymbol{\Phi}}{\partial t} + v_z \frac{\partial \boldsymbol{\Phi}}{\partial z}\right)\right] \Big/ B,$$

where (2) is to be completed with Poisson's equation and equations for the electron dynamics. $\hat{\mathbf{b}}$ is the unit vector in the $\mathbf{B}$ direction. The model (2) evidently ignores finite-Larmor-radius (FLR) effects. By the implicit assumption of homogeneous magnetic fields, we need not explicitly retain a dependence on the magnetic moment in the distribution function.

The second term in $\mathbf{v}_\perp$ is the polarization drift, which originates from the time variation of the $\mathbf{E} \times \mathbf{B}/B^2$ velocity, experienced in the particle frame of reference. This effective acceleration, $\mathbf{g} \sim \partial \mathbf{E}/\partial t \times \mathbf{B}/B^2$, gives rise to a slow particle drift in the $\mathbf{g} \times \mathbf{B}$ direction in or out of the potential well, resulting in a violation of the assumed time-stationarity of the particle distribution. This effect is less pronounced for structures that are strongly $\mathbf{B}$-field aligned, since the observed electric field variation in the particle rest frame is diminished for such structures.

In the limit of large $\mathbf{B}$ fields, i.e. large $\boldsymbol{\Omega}_{ci}$, the polarization contribution to $\mathbf{v}_\perp$ is negligible, and a steady-state solution to (2) is

$$f = F\left(\tfrac{1}{2}Mv_z^2 + e\Phi(\mathbf{r}_\perp, z)\right),$$

with arbitrary $F(\,)$. The $\mathbf{v}_\perp \cdot \boldsymbol{\nabla}_\perp f$ term vanishes identically by $(\boldsymbol{\nabla}\Phi \times \hat{\mathbf{b}}) \cdot \boldsymbol{\nabla}\Phi = 0$. Insertion of the expression for f into Poisson's equation gives

$$\nabla_\perp^2 \Phi + \frac{\partial^2 \Phi}{\partial z^2} = \frac{e}{\epsilon_0}\left[n_e - \int_{-\infty}^{\infty} F\left(\tfrac{1}{2}Mv_z^2 + e\Phi(\mathbf{r}_\perp, z)\right) dv_z\right]. \tag{3}$$

A corresponding expression for $n_e = \int_{-\infty}^{\infty} f_e \, dv_z$ can be obtained similarly where the polarization drift for the electrons can be ignored from the outset. In problems like those considered in the present work, it is assumed that the electrons are isothermally Boltzmann-distributed at all times, $n_e = n_0 \exp(e\Phi/T_e)$, which simplifies the relation between n_e and Φ also in cases where the density n_0 is spatially varying. If $\Phi = \Phi(\mathbf{r}_\perp, z)$ is prescribed then (3) can be considered as an equation for determining F, where F is assumed to be composed of both free and of trapped

https://doi.org/10.1017/S0022377801008947 Published online by Cambridge University Press

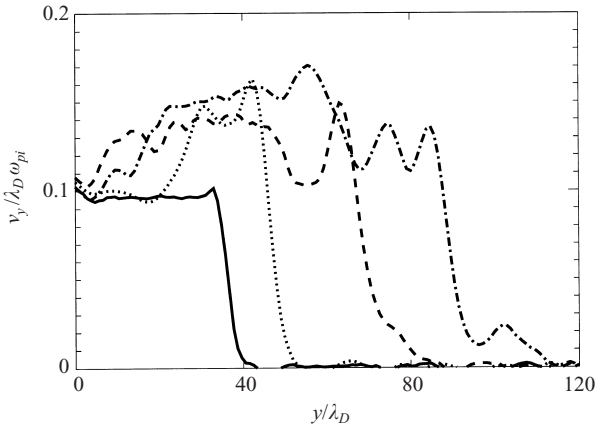


Figure 9. Evolution of the average plasma velocity in the y direction on the symmetry axis, for a case where the ion beam velocity is modulated in the transverse direction by $1.5\,[\,0.75 - 0.25\,\cos(\pi x/D)\,]$, with $2D$ being the beam diameter. The spatial variation is shown for times $t = 0, 10\omega_{pi}^{-1}, 30\omega_{pi}^{-1}$ and $50\,\omega_{pi}^{-1}$.

particle contributions. The $\mathbf{r}_\perp$ dependence of Φ then imposes the $\mathbf{r}_\perp$ variation of F. The class of physically acceptable solutions is restricted by the requirement that distribution functions be positive or zero for all velocities. The solutions are not restricted to cylindrical symmetry. Little is known about the stability of these solutions with respect to two- or three-dimensional perturbations.

The arguments given before explicitly assumed strong magnetic fields. It might be expected that they are applicable also for intermediate field strengths provided the polarization term in $\mathbf{v}_\perp$ is small, i.e. $(v_{T_i}/\Omega_{ci})\boldsymbol{\nabla}_\perp \partial\Phi/\partial z$ is negligible, taking the ion thermal velocity v_{T_i} as representative of v_z. In the extreme case with $\partial\Phi/\partial z = 0$, a cylindrical BGK equilibrium can be obtained trivially, although this limit is not particularly interesting.

Recently, Jovanović and Shukla (2000) have obtained electron–ion vortex solutions in magnetized plasmas, in the form of a 'cylinder' tilted with respect to the magnetic field. These structures can be interpreted as three-dimensional electron holes coupled with hydrodynamic vortices somewhat similar to those studied by Jovanović and Pegoraro (2000).

2.3. Spatially modulated beams

The preceding studies can be understood as dealing with an ion beam that is modulated in space by a step function. We have also investigated the case where the beam has an internal structure. This was obtained by modulating the beam velocity in the transverse direction by a sinusoidal variation having a wavelength corresponding to the beam width. For this case, two basically different cases can be distinguished – one where the beam velocity is maximum in the centre, and one where it reaches its maximum value at the two edges of the beam. We found that the first of these two cases gave rather trivial results, by giving rise to a transverse narrowing of the ion vortices, implying that their formation is controlled by the linearly most unstable central part of the beam.

The other case, with the beam velocity being maximized at the edges, gave some unexpected results. Also here we find that initially the ion vortexes are restricted

https://doi.org/10.1017/S0022377801008947 Published online by Cambridge University Press

to the linearly most unstable region of the beam, implying now that we have two 'vortex chains' on each side of the beam. When these two chains are close enough to allow vortices to merge, we find that the central region that we injected with a reduced velocity is accelerated, implying that the vortices give rise to an enhanced or anomalous viscosity in the direction perpendicular to the beam axis. This effect is illustrated in Fig. 9, showing the spatial variation of the average plasma velocity (average of beam and background) on the symmetry axis at selected times. The overall increase in plasma velocity associated with the formation of phase-space vortices is apparent. The irregularities are correlated with the vortices, i.e. a local maximum of the plasma velocity corresponds closely to a phase-space vortex.

3. Conclusions

In this paper, we have studied the formation and evolution of ion phase-space vortices, generated by an ion beam through a stationary background plasma, by using a 2.5-dimensional numerical particle simulation, assuming Boltzmann-distributed electrons. We have observed the formation of BGK type equilibria for all values of the magnetic field, including $B = 0$, but have found that the lifetime of the structures increases rapidly with increasing magnetic field intensity. It thus seems plausible that the type of two-dimensional structures anticipated by Kato (1976) and Ishibashi and Kitahara (1992) can be formed, but that they are inherently unstable. The simple model (3) derived under the assumption of strong magnetic fields might be applicable also for moderate B fields, as an approximation. Our numerical results indicate that for the plasma parameter range relevant here, the structures are relatively stable in two spatial dimensions when the transverse length scale significantly exceeds the ion Larmor radius and that simultaneously $\boldsymbol{\Omega}_{ci} > \frac{1}{2}\omega_{pi}$. We take this latter inequality as an indication of the necessity to reduce the ion polarization drift, as discussed in Sec. 2.2.1. A generalization of our analysis for the full three-dimensional case would be relevant and interesting, but requires significant computer resources.

The number of relevant parameters for the problem is large, even when, as here, we make the simplifying assumption that both beam and background ions have a Maxwellian distribution. We have as basic parameters the normalized ion beam velocity $V_b/v_{\rm th}$, the density ratio n_b/n_B, temperature ratios T_e/T_i and T_b/T_B, and finally the length or duration of the ion beam. This latter parameter was not considered here, but Pécseli et al. (1984) and Pécseli (1984) demonstrated that ion vortices could also be excited by relatively short ion beams, or bursts. The criterion for the formation of ion holes can for the strongly magnetized case be understood, at least qualitatively, by a linear stability analysis; this case is well approximated by the one-dimensional studies (Sakanaka 1972; Pécseli et al. 1984; Pécseli 1984), and here it has been shown that the phase-space vortices could be interpreted as the saturated stage of the linear ion-beam instability. When a finite-length ion beam was injected, it was found that vortices were also excited in this case, provided that the beam length exceeded the linearly most unstable wavelength. We emphasize that these conclusions are only qualitative; a very strong localized perturbation can also produce ion vortices, but such cases cannot readily be parameterized. For the unmagnetized case, we believe that a linear stability analysis (Fried and Wong 1966) can still serve as a guideline, but in this case, the finite vortex lifetime is no longer easy to quantify, and depends significantly on details of the physical con-

https://doi.org/10.1017/S0022377801008947 Published online by Cambridge University Press

ditions, with several mechanisms being effective at the same time, as our results in Sec. 2.1 demonstrate.

Phase-space vortices are interesting examples of self-organization in highly dynamic, nonlinear systems. By forming well-defined entities, these phase-space structures allow the saturated stage of, for instance, beam instabilities to be described by a modest number of variables, such as the positions, widths and amplitudes of the structures.

We have made certain that the observed vortex lifetimes are not controlled by numerical diffusion. This is also evident from the data in Table 1; the numerical diffusion would be unaffected by the inclusion of a magnetic field, but the numerical results demonstrate a clear increase in lifetime with increasing **B** field.

We believe that the present results could be relevant for interpreting data from the ionospheres and magnetospheres of magnetized planets, such as the Earth. Solitary structures have been observed on spacecrafts; see the summaries by, for example Mälkki et al. (1993) and Eriksson et al. (1997). The origin of these structures was expected to be a nonlinear instability, driven by weak currents, but the data actually speak strongly against this interpretation by showing no preferred direction for the propagation of the observed structures (Mälkki et al. 1993). Indications of the presence of electron phase-space holes were found in the data from the FAST satellite (Ergun et al. 1998). Observations of electrostatic solitary structures in the Earth's magnetotail have been reported from the GEOTAIL satellite (Krasovsky et al. 1997; Omura et al. 1999). It is plausible that also these can be interpreted in terms of phase-space structures, although a significant amount of work remains to be done concerning the derivation of an actual spatial structure, which in the experiments has to be deduced from a time-varying signal obtained from the potential difference between two probes with large separation, on the moving spacecraft. It will be interesting to see whether the data from the CLUSTER satellites will reveal signatures of plasma solitary structures. In this case, the spatial resolution of these satellites will offer a good possibility for determining conditions for the occurrence of such structures.

Acknowledgement

This work was supported in part by the Norwegian Research Council.

Appendix. Outline of the numerical code

In this appendix, we describe central parts of the numerical code used for the simulations. The part for particle motion is fairly standard (Birdsall and Langdon 1985), and we will here discuss only the method for solving the nonlinear Poisson equation.

In the present study, the Poisson equation takes the form

$$\nabla^2\phi = -\rho + e^{\phi/T_e}, \tag{A 1}$$

in terms of dimensionless variables. The exponential term arises from the assumption of Boltzmann-distributed electrons. The electron temperature is made dimensionless by a properly chosen reference temperature referring to the ion population. Solution of (A 1) implies solving a nonlinear elliptic partial differential equation on a mesh of typically several hundred grid points in each direction. The degree of nonlinearity depends on the ion density and the electron temperature.

https://doi.org/10.1017/S0022377801008947 Published online by Cambridge University Press

Initially, this problem was solved using a standard Gauss–Seidel iterative finite-difference method with odd–even ordering (Flannery et al. 1992). If h_x and h_y denote the grid spacings in the x- and y-directions, respectively, the iteration scheme for this Poisson solver can be written as

$$\phi_{i,j}^{\mathrm{new}} = \tilde{\phi}_{i,j} + \frac{h_x^2 h_y^2}{2(h_x^2 + h_y^2)}(\rho - e^{\phi_{i,j}^{\mathrm{old}}/T_e}), \tag{A 2}$$

where

$$\tilde{\phi}_{i,j} = \frac{h_y^2}{2(h_x^2 + h_y^2)}(\phi_{i+1,j} + \phi_{i-1,j}) + \frac{h_x^2}{2(h_x^2 + h_y^2)}(\phi_{i,j+1} + \phi_{i,j-1})\,. \tag{A 3}$$

To increase the efficiency, the solver also made use of the multigrid approach. This was done by first solving the problem on a coarser grid to obtain an approximate solution. This solution was then interpolated onto a finer grid before new iterations were performed. Unfortunately, this approach gave rise to numerical instabilities when relatively low electron temperatures were combined with a fairly large grid spacing. One might think that this problem could be avoided by making the first few iterations on the finest grid, before doing the major part of the computational work on a coarser grid. This was not the case. The occurrence of the instabilities depended solely on the electron temperature and the grid spacing, and to a smaller extent on the ion density. The stability did not depend significantly on how close the starting point of the iteration was to the correct solution.

In order to make the multigrid iteration scheme more stable, the scheme itself had to be modified. The potential occurring in the exponential term in (A 2) was therefore changed from $\phi_{i,j}^{\mathrm{old}}$ to $\tilde{\phi}_{i,j}$, thus removing the direct dependence of $\phi_{i,j}^{\mathrm{new}}$ on $\phi_{i,j}^{\mathrm{old}}$. The modified iteration scheme thus became

$$\phi_{i,j}^{\mathrm{new}} = \tilde{\phi}_{i,j} + \frac{h_x^2 h_y^2}{2(h_x^2 + h_y^2)}(\rho - e^{\tilde{\phi}_{i,j}/T_e}), \tag{A 4}$$

where $\tilde{\phi}_{i,j}$ is as defined in (A 3).

To justify the modifications made to the standard iteration scheme, an idealized case was analysed. Assuming the plasma density to be perfectly homogeneous and equal to ρ_0, and also choosing the grid spacing to be the same in both directions and equal to h, the iterative scheme for the even and odd grid points respectively can be written as

$$\phi_t^e = \phi_{t-1}^o + \tfrac{1}{4}h^2(\rho_0 - e^{\phi_{t-1}^e/T_e}), \tag{A 5}$$

$$\phi_t^o = \phi_t^e + \tfrac{1}{4}h^2(\rho_0 - e^{\phi_{t-1}^o/T_e}). \tag{A 6}$$

The exact solution to this problem, to which the iterative solution should converge, is found trivially to be given as $\phi_\infty = T_e \ln \rho_0$. In the current example, the electron temperature T_e was chosen to be equal to unity and the density ρ_0 was set equal to 1.3 times the equilibrium density. In Figs A.1 and A.2, it can be seen how the two iteration schemes performed for different values of the grid spacing h in solving this idealized problem. The potential at the even and odd grid points is normalized against the exact solution shown as a function of the number of iterations. Comparing the plots in the two figures, one can see that the oscillating

https://doi.org/10.1017/S0022377801008947 Published online by Cambridge University Press

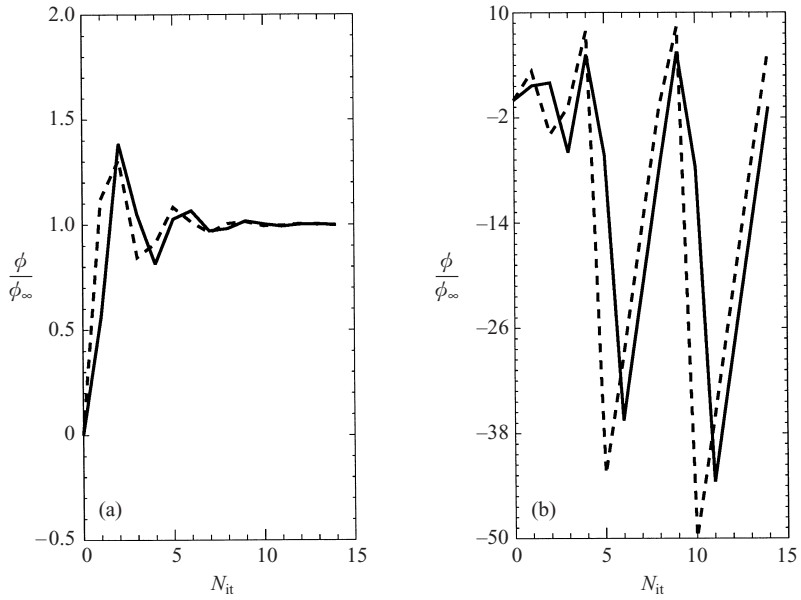


Figure A.1. Stability tests of the Poisson solver with $T_e = 1$ and $\rho_0 = 1.3$, using a standard odd–even Gauss–Seidel iteration: (a) $h = 1.4$; (b) $h = 2.4$. The solid and dashed lines represent the potential at even and odd grid points, respectively.

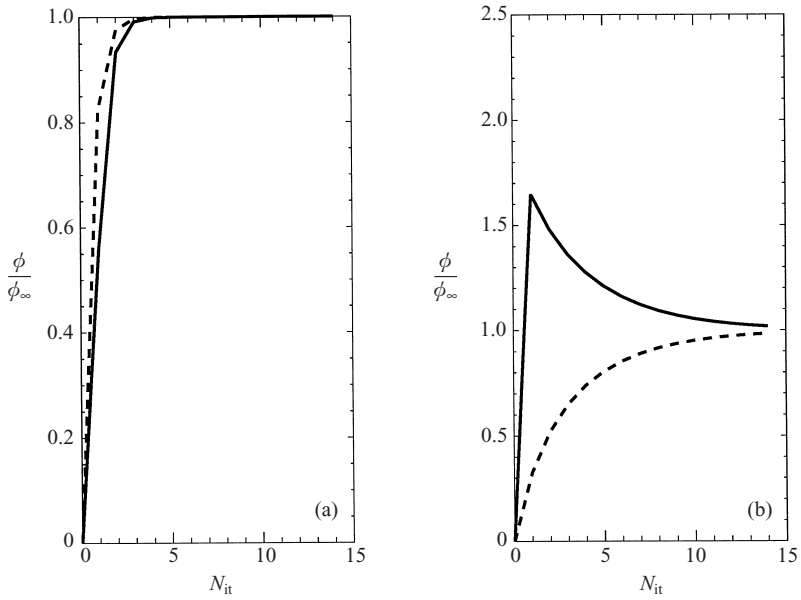


Figure A.2. Stability tests of the Poisson solver with $T_e = 1$ and $\rho_0 = 0.3$, using the modified iteration scheme. (a) $h = 1.4$; (b) $h = 2.4$. The solid and dashed lines represent the potential at even and odd grid points, respectively.

behaviour of the solution produced by the standard iteration scheme occurring for $h > 1$ is not present in the corresponding solution of the modified iteration scheme. In fact, further tests both on this simplified problem and on more realistic problems suggested that the maximum grid spacing, corresponding to the coarsest grid in the

https://doi.org/10.1017/S0022377801008947 Published online by Cambridge University Press

multigrid procedure, can be increased by approximately 40% by using the modified iteration scheme.

The reason for the improved performance of the modified iteration scheme is that $\tilde{\phi}_{i,j}$, now also occurring in the exponential term of (A 4), represents a mean potential level at the neighbouring grid points. In this way, numerical oscillations experienced in the results from the standard iteration scheme can be removed. This modified iteration scheme could therefore perform satisfactorily in a multigrid algorithm to produce an accurate and efficient solver of the nonlinear Poisson equation.

References

Berk, H. L., Nielsen, C. E. and Roberts, K. V. 1970 *Phys. Fluids* **13**, 980.

Bernstein, I. B., Green, J. M. and Kruskal, M. D. 1957 *Phys. Rev.* **108**, 546.

Birdsall, C. K. and Langdon, A. B. 1985 *Plasma Physics via Computer Simulation*. McGraw-Hill, New York.

Chan, C., Cho, M., Hershkowitz, N. and Intrator, T. 1984 *Phys. Rev. Lett.* **52**, 1782.

Ergun, R. E., Carlson, C. W., McFadden, J. P., Mozer, F. S., Muschietti, L. and Roth, I. 1998 *Phys. Rev. Lett.* **81**, 826.

Eriksson, A. I., Mälkki, A., Dovner, P.-O., Boström, R., Holmgren, G. and Holback, B. 1997 *J. Geophys. Res.* **102**, 11 385.

Fijalkow, E. 1999 *J. Plasma Phys.* **61**, 65.

Flannery, B. P., Press, W. H., Teukolsky, S. A. and Vetterling, W. T. 1992 *Numerical Recipes in C*, 2nd edn. Cambridge University Press.

Fried, B. D. and Wong, A. Y. 1966 *Phys. Fluids* **9**, 1084.

Grésillon, D. and Doveil, F. 1975 *Phys. Rev. Lett.* **34**, 77.

Huld, T., Pécseli, H. L. and Rasmussen, J. J. 1990 *IEEE Trans. Plasma Sci.* **18**, 149.

Ikezi, H., Kamimura, T., Kako, M. and Lonngren, K. E. 1973 *Phys. Fluids* **16**, 2167.

Ishibashi, N. and Kitahara, K. 1992 *J. Phys. Soc. Jpn* **61**, 2795.

Johnsen, H., Pécseli, H. L. and Trulsen, J. 1985 *Phys. Rev. Lett.* **55**, 2297.

Johnsen, H., Pécseli, H. L. and Trulsen, J. 1987 *Phys. Fluids* **30**, 2239.

Jovanović, D. and Pegoraro, F. 2000 *Phys. Rev. Lett.* **84**, 95.

Jovanović, D. and Shukla, P. K. 2000 *Phys. Rev. Lett.* **84**, 4373.

Kako, M., Taniuti, T. and Watanabe, T. 1971 *J. Phys. Soc. Jpn* **31**, 1820.

Kato, K. 1976 *J. Phys. Soc. Jpn* **41**, 1050.

Kiwamoto, Y. 1974 *J. Phys. Soc. Jpn* **37**, 466.

Kofoed-Hansen, O., Pécseli, H. L. and Trulsen, J. 1989 *Physica Scripta* **40**, 681.

Krasovsky, V. L., Matsumoto, H. and Omura, Y. 1997 *J. Geophys. Res.* **102**, 22 131.

Lynov, J. P., Michelsen, P., Pécseli, H. L., Rasmussen, J. J., Saéki, K. and Turikov, V. 1979 *Physica Scripta* **20**, 328.

Mälkki, A., Eriksson, A. I., Dovner, P.-O., Boström, R., Holback, B., Holmgren, G. and Koskinen, H. 1993 *J. Geophys. Res.* **98**, 15 521.

Morse, R. L. and Nielson, C. W. 1969 *Phys. Rev. Lett.* **23**, 1087.

Nakamura, Y., Bailung, H. and Shukla, P. K. 1999 *Phys. Rev. Lett.* **83**, 1602.

Nicholson, D. R. 1983 *Introduction to Plasma Theory*. Wiley, New York.

Omura, Y., Kojima, H., Miki, N., Mukai, T., Matsumoto, H. and Anderson, R. 1999 *J. Geophys. Res.* **104**, 14 627.

Oppenheim, M., Newman, D. L. and Goldman, M. V. 1999 *Phys. Rev. Lett.* **83**, 2344.

Pécseli, H. L. 1984 In: *Proceedings from the Second Symposium on Plasma Double Layers and Related Topics, University of Innsbruck*, (ed. R. Schrittwieser and G. Eder), p. 81. Studia, Innsbruck.

Pécseli, H. L. and Trulsen, J. 1982 *Phys. Rev. Lett.* **48**, 1355.

Pécseli, H. L., Trulsen, J. and Armstrong, R. 1981 *Phys. Lett.* **81A**, 386.

Pécseli, H. L., Trulsen, J. and Armstrong, R. 1984 *Physica Scripta* **29**, 241.

https://doi.org/10.1017/S0022377801008947 Published online by Cambridge University Press

Saéki, K. 1973 *J. Phys. Soc. Jpn* **35**, 251.
Saéki, K., Michelsen, P., Pécseli, H. L. and Rasmussen, J. J. 1979 *Phys. Rev. Lett.* **42**, 501.
Sakanaka, P. H. 1972 *Phys. Fluids* **15**, 1323.
Schamel, H. 1982 *Phys. Lett.* **89A**, 280.
Schamel, H. 1986 *Phys. Rep.* **140**, 161.
Terry, P. W., Diamond, P. H. and Hahm, T. S. 1990 *Phys. Fluids* **B2**, 2048.
Turikov, V. 1984 *Physica Scripta* **30**, 73.

https://doi.org/10.1017/S0022377801008947 Published online by Cambridge University Press